



# Thermal monitoring of lithium-ion batteries based on machine learning and fibre Bragg grating sensors

Transactions of the Institute of  
Measurement and Control  
1–9

© The Author(s) 2023



Article reuse guidelines:

[sagepub.com/journals-permissions](https://sagepub.com/journals-permissions)

DOI: 10.1177/01423312221143776

[journals.sagepub.com/home/tim](https://journals.sagepub.com/home/tim)Shiyun Liu  and Kang Li 

## Abstract

Lithium-ion batteries (LiBs) are well-known power sources due to their higher power and energy densities, longer cycle life and lower self-discharge rate features. Hence, these batteries have been widely used in various portable electronic devices, electric vehicles and energy storage systems. The primary challenge in applying a Lithium-ion battery (LiB) system is to guarantee its operation safety under both normal and abnormal operating conditions. To achieve this, temperature management of batteries should be placed as a priority for the purpose of achieving better lifetime performance and preventing thermal failures. In this paper, fibre Bragg Grating (FBG) sensor technology coupling with machine learning (ML) has been explored for battery temperature monitoring. The results based on linear and nonlinear models have confirmed that the novel methods can estimate temperature variations reliably and accurately.

## Keywords

Lithium-ion battery thermal management, FBG sensor, fast recursive algorithm, linear/nonlinear model

## Introduction

Lithium-ion batteries (LiBs) are one of the most promising energy storage techniques in power systems and mobile facilities by virtue of its higher power and energy densities, longer cycle life and lower self-discharge rate qualities (Kang et al., 2014). These features are highly suitable for various types of portable electronics devices, electrical vehicles (EV), energy storage applications, aircrafts and even aerospace applications (Li et al., 2020, 2021). However, the extensive applications are usually operated under a wide range of extreme environments, like high-altitude/latitude, elevated temperatures and high charge/discharge rates (Richardson, 2016). This is likely to cause a series of issues in battery thermal management.

For instance, when the environment temperature is below 0°C, the depth of discharge (DoD) and the power output of the battery decrease significantly (Xie et al., 2022). However, operating at high temperatures (40°C) will also accelerate the chemical or mechanical reaction happening between electrolyte and the electrodes (Amine et al., 2005). In this case, solid electrolyte interphase (SEI) will be formed, which leads to the impedance increase at the anode and active lithium reduction in the battery (Liu et al., 2020). Furthermore, the decomposition of electrolyte results in active lithium loss. The aforementioned aging mechanisms lead to capacity fade (Liu et al., 2020). If the generated heat cannot be sufficiently dissipated, the battery internal temperature goes beyond the acceptable scope rapidly and then results in a great many exothermic events within the battery, such as fires, venting and electrolyte leakage (Feng et al., 2015; Liao et al., 2019). Moreover, the nonuniform thermal distribution inside the battery will result

in the issues of inconsistent electrochemical processes and thus decrease the battery pack cycle life (Olabi et al., 2022). In this sense, maintaining the operating temperature of battery under safe and optimal conditions is extremely important. It is necessary to monitor and predict temperature variations through a reliable and effective method.

The conventional ways to detect the thermal features are to use flexible thin-film thermocouples (TFTCs) (Li et al., 2013) or micro-thin-film resistance temperature detectors (RTD) (Lee et al., 2011) attached to the surface or embedded into battery cores. These methods suffer from various limitations, such as vulnerability corroded by internal/external environment, complex to operate and low accuracy of detection (Lee et al., 2011). In contrast, electrochemical impedance spectroscopy (EIS) (Barsoukov and Macdonald, 2005) exhibits the advantages that no temperature sensors are required, thermal measurements are short and the measured battery cells are non-destructive while indicating the internal and external temperature of LiBs. At the same time, the sensorless methods also face the challenges of State of Charge (SoC) and ageing dependence on the impedance, measuring parameters crosstalk interference and operation frequency selection (Raijmakers et al., 2019). Johnson noise thermometry (JNT) method (Edler and Seefeld, 2015) is an appropriate

School of Electronic and Electrical Engineering, University of Leeds, UK

## Corresponding author:

Kang Li, School of Electronic and Electrical Engineering, University of Leeds, Woodhouse Lane, Leeds LS2 9JT, UK.

Email: K.Li1@leeds.ac.uk

candidate for measuring temperature that the applications working in a harsh environment (e.g. nuclear reactors). Nonetheless, there are relatively large errors in measuring the surface temperature of a battery pack when it is coupled with a giant magnetoresistance (GMR) sensor and a K-type thermocouple (Raijmakers et al., 2019).

In recent years, the methods for battery temperature monitoring based on various optical fibre sensing techniques have been explored (Han et al., 2021). For instance, with the assistance of optical fibre sensors, Yu et al. (2022) used the Rayleigh scattering approach to decode the internal temperature and strain evolution of a pouch battery cell. Wei et al. (2022) presented a method for real-time temperature distribution measurement by implanting the distributed fibre optical sensor (DFOS) into a battery cell. The configured smart cell can achieve a real-time distributed sensing of the temperature matrix with a high spatial resolution of 2.6 mm. Yang et al. (2022) proposed a distributed thermometry method using optical frequency domain reflectometry (OFDR). The technique was demonstrated on a three-cell pouch-type battery pack. The experimental results indicated that the sensor can simultaneously measure temperature distribution of multiple battery cells.

Particularly, fibre Bragg grating (FBG) sensors have been extensively investigated and used in monitoring battery thermal variations because the Bragg wavelength favourably shifts linearly with temperature under certain conditions (Han et al., 2021; Wei et al., 2021). Additionally, FBG sensor is superior to conventional thermal sensors in terms of its electricity immunity, high sensitivity, multiplexing, and the possibility of the integration inside the batteries. (Nascimento et al., 2017; Raijmakers et al., 2019).

Yang et al. (2013) initiated the investigation of optical fibre Bragg grating (FBG) sensors in LiBs to measure external temperature variations under normal (discharged at various current) and abnormal conditions (overcharge and external short-circuit). The results showed the FBG sensors have faster thermal response in comparison with the thermocouples. Moreover, this method can be also employed to detect temperature distribution of battery stack. Following this research, a number of experiments have been conducted in terms of the technical reliability and measurement complexity. For instance, Meyer et al. (2015) investigated the advantages of FBGs for enhanced battery safety by several different experiments. First, with the FBG sensor network, the temperature of each cell was recorded during fast charging, which showed FBG sensors can detect the maximum temperature more accurately than the thermistors. Second, the characteristic volume behaviour of LiBs was detected precisely by FBG sensors, although the sensors did not show a clearly detectable aging under nominal and accelerated conditions. In addition, it was found that the sensitivity of the FBG strain sensor is much higher (around 50 times) than the sensitivity of the temperature sensor. These results show that the FBG sensor application offers an alternative approach to avoid thermal runaway. Likewise, Nascimento et al. (2017) made a comparative study using FBG sensors and thermocouples to monitor battery thermal variations in real-time at three different battery locations (top, middle and bottom) under both constant current charge and various discharge

rates (0.53 C, 2.67 C and 8.25 C) conditions. They found the responses of the two types of sensors under lower C-rates are closer to each other, whereas FBG sensors under abuse conditions (higher discharge rate) showed rapid response to the heat generation in all locations.

Furthermore, FBG sensors for permanent and immediate monitoring of the internal temperature were also studied. For instance, Schwartz et al. (2015) explored to use a single FBG sensor embedded directly into the electrode stack of lithium-ion pouch cells, which detected both mechanical strain from lithium-ion insert into the electrodes and thermal strain from temperature variations under normal charge-discharge conditions. At the same time, another FBG sensor without experiencing the mechanical strain was loosely attached to the top of cell surface as a temperature reference sensor to decouple the intercalation mechanical strain from the embedded FBG signal. The research showed signals obtained from the internal sensors were stronger (over four times) than those detected from external sensors of the pouch. Similarly, Novais et al. (2016) conducted research on measuring internal and external temperature variations through four FBG sensors during different C-rates. In their experiment, two FBG sensors were inserted between two separators layers, that is, at the centre of the electrochemically active site and near the tab-electrode connection. Meanwhile, another two external sensors were placed on the surface of the pouch cell, parallel to the above internal sensors. The study also indicated the observed external temperature variations were significantly lower than the internal temperature (e.g.  $1.5^{\circ}\text{C} \pm 0.1^{\circ}\text{C}$  and  $4.0^{\circ}\text{C} \pm 0.1^{\circ}\text{C}$  for external and internal, in order). Apart from this, they found that the external sensor's signal was slightly delayed compared with the internal signal. Fleming et al. (2018) and Fortier et al. (2017) also reported the temperature differences between internal and surface of LiBs, with about  $10^{\circ}\text{C}$  during discharge and  $3^{\circ}\text{C}$  during charge phase, respectively. More importantly, they found that utilizing FBG sensor to monitor battery internal thermal characteristics has a negligible impact upon the battery performance.

However, the aforementioned studies were conducted under ambient temperatures. Considering the wide range of practical working environments of battery-driven facilities (e.g. EVs), Nascimento et al. (2019) further proposed an FBG-based sensor network for monitoring the surface temperature of LiB in a smartphone under dry, temperate and cold environments, at constant charge and different discharge rates (1.32 C, 2.67 C and 5.77 C). In this experiment, it is interesting to note that five different spots of battery surface were monitored both in situ and in operando only using a single optical fibre. The results confirmed that the FBG sensor network is a precise and useful tool that can be employed to monitor the temperature variations of LiBs. More specifically, the thermal mapping demonstrated that the detected highest temperature was at the top of the battery (near of the electrodes), followed by the top-middle position. The temperature at the middle-bottom was slightly higher than that at the middle. The lowest temperature in all cases was detected at the bottom of the battery. These findings offered strong evidence for an effective cooling system design. Zhang et al. (2022) proposed a novel data-driven-based FBG sensor temperature

calibration method that can achieve desirable estimation results under a wide range of environments. These make the FBG-based temperature monitoring methods more friendly to use in more real-life applications.

In summary, it can be concluded that the existing FBG sensor-based battery temperature measurement studies have demonstrated the great potential of FBG sensors in LiB temperature management, given their advantages such as rapid response and precise measurement under both normal and abnormal conditions. However, the aforementioned research on FBG-based temperature monitoring methods is still at a nascent stage. Using FBG sensors attached to the surface of battery or inserted into battery cell alone is not sufficient to monitor the battery states in full. Battery temperature estimation models still play a key role in keeping battery safety. Among the common battery thermal estimation models (Jiang et al., 2022; Karimi et al., 2022; Mahamud and Park, 2022), machine learning (ML) can be utilized to efficiently estimate the temperature variations of LiBs (Liu et al., 2018) as ML does not need the knowledge or data of the internal characteristics of the batteries (Li et al., 2022) and is able to learn the linear and/or nonlinear system dynamics.

In this paper, we explore to combine the wavelength of FBG sensors and battery working parameters with ML to monitor LiB surface temperature. In detail, multiple sensor signals, terminal voltage, battery current and surface temperature are obtained from a lab experimental setup. Then, a linear method and a nonlinear data-driven method are developed. The input terms with the maximum contributions are selected first by a fast recursive algorithm (FRA; Li et al., 2005). Then two data-driven models are constructed, and temperature estimation has been achieved by FRA-linear and FRA-nonlinear models separately. Finally, based on the experimental results, the battery thermal estimation performance under two different models is compared.

The remainder of the paper is organized as follows. Section ‘Preliminaries’ provides the details of the FBG sensor, linear/nonlinear modelling methods and the FRA. The experimental setup, the two-stage data-driven methods, and the estimation results are detailed in section ‘Simulation results and discussion’. Finally, section ‘Conclusion and future work’ concludes the paper and the future research is also discussed.

## Preliminaries

### FBG sensor

FBG sensor is an optical filtering device which enables a particular wavelength of the light spectrum to be reflected back while the remaining part is transmitted nearly without being affected (Raijmakers et al., 2019). The wavelength of the reflected signal is named as the Bragg wavelength  $\lambda_B$ , which has the following relationship (Morey et al., 1990)

$$\lambda_B = 2n\Lambda_G \quad (1)$$

where  $n$  is the effective index of the refraction and  $\Lambda_G$  is the grating pitch between the grating planes.

### Linear model

The linear model assumes that the linear relationship between the independent input variables  $X_i$  and a single dependent variable  $Y$  (Ravishanker et al., 2021). Linear models are among the most popular models in analysing the experimental data. The general function for a linear model is

$$Y = \beta_0 + \sum \beta_i X_i + \epsilon_i \quad (2)$$

where  $\beta$  is linear parameter estimates to be computed and  $\epsilon$  represents the error terms.

### Nonlinear model

A nonlinear model describes nonlinear relationship between the dependent variable  $Y$  as a function of a combination of nonlinear parameters and independent variables  $X_i$ . The parameters can take the forms of an exponential, trigonometric, power or any other nonlinear function (MathWorks, 2022). In order to estimate the nonlinear parameters, an iterative algorithm is generally used

$$Y = f(X_i, \beta) + \epsilon_i \quad (3)$$

where  $\beta$  is linear parameter estimates to be computed and  $\epsilon$  represents the error terms.

### FRA

FRA (Li et al., 2005) can solve the least-squares problem recursively without the need for matrix deposition and transformation. Therefore, the method is efficient in constructing both model structure and calculate model parameters. In this work, the FRA is used to select the most relevant inputs and determine the parameters for linear and nonlinear models.

First, the FRA is introduced by defining a recursive matrix  $M_k$  and a residual matrix  $R_k$

$$\begin{cases} M_k = P_k^T P_k, & k = 1, \dots, n \\ R_k = I - P_k M_k^{-1} P_k^T, & R_0 = I \end{cases} \quad (4)$$

where  $P_k \in \mathbb{R}^{N \times k}$  contains the first  $k$  selected regressors (or model terms) out of the full regression matrix.

Second, suppose  $\{p_i, i = 1, \dots, n\}$  in  $P$  are linearly independent mutually, we combine the definition in (4), the recursive matrix  $R_k, k = 1, \dots, n$ , therefore has the following properties

$$R_k^T = R_k, (R_k)^2 = R_k \quad (5)$$

$$R_k R_j = R_j R_k = R_k, k \geq j \quad (6)$$

$$R_k p_i = 0, \forall i \in \{1, \dots, k\} \quad (7)$$

$$R_{k+1} = R_k - \frac{R_k p_{k+1} p_{k+1}^T R_k}{p_{k+1}^T R_k p_{k+1}}, k = 0, 1, \dots, n-1 \quad (8)$$

Suppose  $E_k$  is the square error after selecting  $k$  terms (Liu et al., 2018), and it can be expressed as

$$E_k = \mathbf{y}^T \mathbf{R}_k \mathbf{y} \quad (9)$$

From equations (8) and (9), the  $E_{k+1}$  can be expressed after adding the  $(k+1)$ th item

$$\left. \begin{aligned} E_{k+1} &= \mathbf{y}^T \mathbf{R}_{k+1} \mathbf{y} = E_k - \frac{\mathbf{y}^T \mathbf{R}_k \mathbf{p}_{k+1} + \mathbf{p}_{k+1}^T \mathbf{R}_k^T \mathbf{y}}{\mathbf{p}_{k+1}^T \mathbf{R}_k \mathbf{p}_{k+1}} \mathbf{y} \\ E_0 &= \mathbf{y}^T \mathbf{y} \end{aligned} \right\} \quad (10)$$

Moreover, defining

$$\left. \begin{aligned} p_i^{(k)} &\triangleq \mathbf{R}_k p_i, p_i^{(0)} \triangleq \mathbf{R}_0 p_i = p_i \\ i &= 1, \dots, n, k = 0, 1, \dots, n \end{aligned} \right\} \quad (11)$$

From equations (5)–(7), equation (11) can become as

$$\Delta E_{k+1} = - \frac{(\mathbf{y}^T p_{k+1}^{(k)})^2}{(\mathbf{p}_{k+1}^{(k)})^T p_{k+1}^{(k)}}, k = 0, \dots, n-1 \quad (12)$$

Equation (12) shows the net contribution of term  $p_{k+1}$  to the cost function when it is included in the model.

In order to simplify the computational complexity, two new quantities are defined

$$\left. \begin{aligned} a_{k,i} &\triangleq (p_k^{(k-1)})^T p_k^{k-1}, a_{1,i} \triangleq p_1^T p_i \\ a_{k,y} &\triangleq (p_k^{(k-1)})^T \mathbf{y}, a_{1,y} \triangleq (p_1^0)^T \mathbf{y} = p_1^T \mathbf{y} \\ i &= k, \dots, n, k = 1, 2, \dots, n \end{aligned} \right\} \quad (13)$$

Based on equations (5)–(7) and equation (11), the following equation can be produced

$$\left. \begin{aligned} a_{k,i} &= p_k^T p_i - \frac{\sum_{j=1}^{k-1} (a_{j,k} a_{j,i})}{a_{j,j}} \\ k &= 1, \dots, n, i = k, \dots, n \end{aligned} \right\} \quad (14)$$

$$a_{k,y} = p_k^T \mathbf{y} - \frac{\sum_{j=1}^{k-1} (a_{j,k} a_{j,y})}{a_{j,j}}, k = 1, \dots, n \quad (15)$$

From equation (15), we can get

$$\mathbf{y}^T p_i^{(k)} = \mathbf{y}^T p_i - \frac{\sum_{j=1}^k (a_{j,y} a_{j,i})}{a_{j,j}} \quad (16)$$

Similarly, from equation (14), it can be derived

$$(p_i^{(k)})^T p_i^{(k)} = (p_i)^T p_i - \sum_{j=1}^k \left( \frac{a_{j,i}^2}{a_{j,j}} \right) \quad (17)$$

Finally, by substituting equations (16) and (17) into equation (12), the net contribution of  $p_{k+1}, k = 0, 1, \dots, n-1$  to the cost function can be shown explicitly as following

$$\Delta E_{k+1} = - \frac{(\mathbf{y}^T p_{k+1} - \sum_{j=1}^k \left( \frac{a_{j,y} a_{j,k+1}}{a_{j,j}} \right))^2}{(\mathbf{p}_{k+1})^T p_{k+1} - \sum_{j=1}^k \left( \frac{a_{j,k+1}^2}{a_{j,j}} \right)} \quad (18)$$

Equation (18) gives the fast algorithm for explicitly computing the net contribution of a selected model term. After selecting the model terms, the model parameter can be computed recursively using

$$\hat{w}_j = \left( a_{j,y} - \sum_{i=j+1}^k \hat{w}_i a_{j,i} \right) / a_{j,j}, j = k, k-1, \dots, 1 \quad (19)$$

## Simulation results and discussion

### Experimental setup

A schematic diagram of the experimental setup for thermal monitoring of the LiB is shown in Figure 1. In the work, a commercial cylindrical LiB cell (18650 LiFePO<sub>4</sub>, 3.2 V, 1.6 Ah) was used. On the preset of the experiment, three FBG sensors were glued to the cell surface. Each of the two adjacent sensors had a slightly different orientation (the angle of the adjacent two sensors is about 45°). The central wavelength for each FBG sensor is 1534, 1539 and 1544 nm, respectively. The sensors signal was obtained by a Micron-Optics SM-130 interrogator. In addition, one thermocouple sensor was also attached to the cell whose position is closed to the FBG sensors, to detect the battery shell temperature (T), thus making it as a reference temperature. For the modeling purpose, in this study, the temperature gradient on the surface of the battery where the sensors are collocated is assumed to be uniform. The terminal voltage (V) and battery current (I) of the cell were measured by a NEWARE BTS 4000 battery test system. All the equipment was set at a 1 Hz sampling frequency for data measurements.

The whole process of the experiment was conducted under an ambient temperature. The tested cell was operated at the cycle of a constant-current constant-voltage (CC-CV) charging process and a constant-current (CC) discharging process. Specifically, the cell was charged under a CC of 1.6 A until the terminal voltage reached 3.6 V upper cut-off voltage. Then, the cell was charged under CV until the current decreased by near 75 mA. Between the charging and discharging phases, 10 minutes were also set as a resting time. After that, the cell was discharged under CC of 1.6 A until the lower 2.0 V cut-off voltage was reached. There were 30 complete charging and discharging cycles in total. The six data

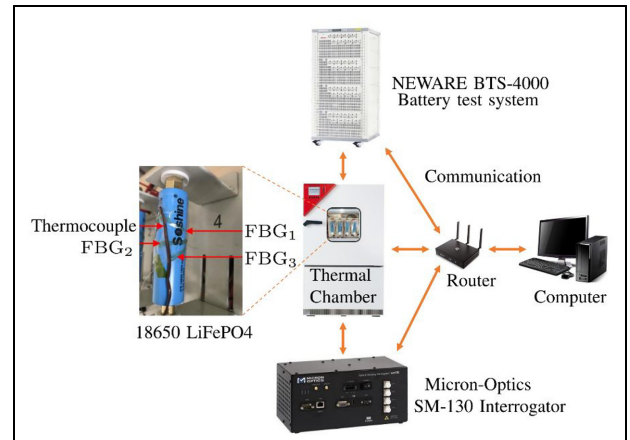
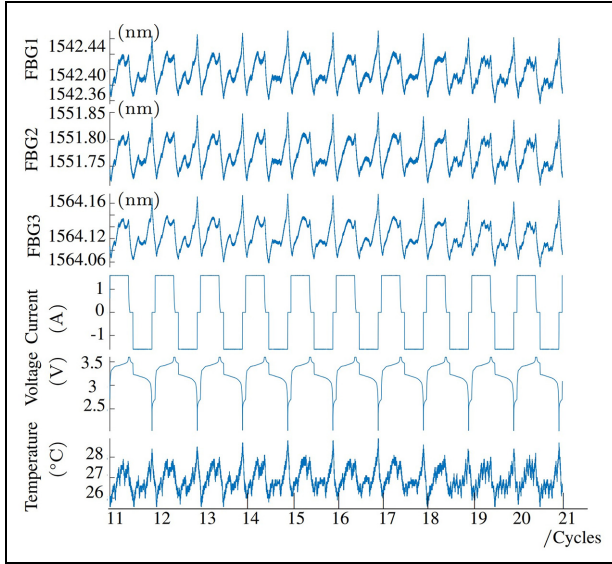


Figure 1. Schematic diagram for thermal monitoring of the lithium-ion battery.



**Figure 2.** Training and testing data in the project, cycles 11–20. Training data: cycles 11–15; testing data: cycles 16–20.

measurements (FBG<sub>1</sub>, FBG<sub>2</sub>, FBG<sub>3</sub>, current, voltage and temperature) for the next modelling structure were obtained during the charging–discharging cycles.

### Data collection

In the work, cycles of (11 – 15) contained (42, 592 × 6) data points including data of FBG<sub>1</sub>, FBG<sub>2</sub>, FBG<sub>3</sub>, current, voltage and temperature are used for model training, while another (42, 592 × 6) data points from the cycles of (16 – 20) were used for model validation, as shown in Figure 2. It is evident that the measured peak wavelength shifts from the FBG sensors agree well with the temperature data measured via the thermocouple. In addition, both of the FBG wavelength shifts and battery temperature have a close relationship with the changes of battery charge/discharge current and terminal voltage.

### Data-driven models

Considering the necessity of higher accuracy and working efficiency for battery temperature estimation, a two-part data-driven method is developed in this paper, as shown in Figure 3. The first part is based on the FRA, which is mainly used to select the proper model terms for the purpose of reducing the computational cost and avoiding the over-fitting problems (Liu et al., 2018); FRA is capable of ranking the significance of the signals from the FBG sensors based on their correlations with the temperature measured by the thermal couple. Another function of FRA is to construct the linear and nonlinear models for battery external temperature estimation. The linear and nonlinear models can build linear and nonlinear relationships between the FBG wavelength shifts and the temperature as well as the choosing battery model working parameters. The detailed procedure to

determine the significant terms and corresponding weights of linear/nonlinear models are shown as follows:

1. Generating the candidate model term pool which contains the aforementioned measurements: FBG<sub>1</sub>, FBG<sub>2</sub>, FBG<sub>3</sub>, current (I), voltage (V) and temperature.
2. Calculating the net contribution of model terms and choosing the most significant one using equation (18).
3. The procedure is repeated until no more significant cost function reduction can be achieved.
4. After selecting the appropriate model terms, calculate the model parameters using equation (19).

Based on the first part of calculation results, the linear and nonlinear data-driven methods can be constructed respectively.

In order to evaluate the performance of the two models, two different performance metrics are introduced. The first is the mean squared error (MSE) for the temperature estimation. It is defined as

$$MSE = \frac{1}{n} \sum_{i=1}^n (Y_i - \hat{Y}_i)^2 \quad (20)$$

where  $Y_i$  is the temperature measured by the thermocouple and  $\hat{Y}_i$  are the estimation values based on the linear/nonlinear models.  $n$  denotes the number of data samples used for model training/testing.

The second metric is the mean absolute error (MAE), which is calculated as the sum of absolute errors between the observed temperature and predicted temperature divided by the total number of samples used for model training or model testing

$$MAE = \frac{\sum_{i=1}^n |Y_i - \hat{Y}_i|}{n} \quad (21)$$

where  $Y_i$  is the true value and  $\hat{Y}_i$  is the prediction.  $n$  is the number of data samples used for modelling.

**FRA-linear model.** In the linear model, the term pool is

$$X_{I \text{ term pool}} = [FBG_1, FBG_2, FBG_3, I, V]^T \quad (22)$$

While the model terms selected by FRA in the first stage is

$$X_I = [FBG_2, FBG_1, V, FBG_3]^T \quad (23)$$

$Y_{\text{train}}$  is the battery surface temperature detected by a thermocouple.

It is worth noting that the time spent on training using FRA for the linear model is 0.1094 seconds. Table 1 illustrates the training results and testing error using the FRA-linear model. It is shown that the MSE for both the training and testing is only 0.0460 and 0.0514, respectively. The MAE for both the training and testing are 0.1684 and 0.1866 in order.

Figure 4 illustrates the temperature estimated by the FRA-linear model. The blue line is the battery surface temperature measured by the thermocouple, and the yellow line is the

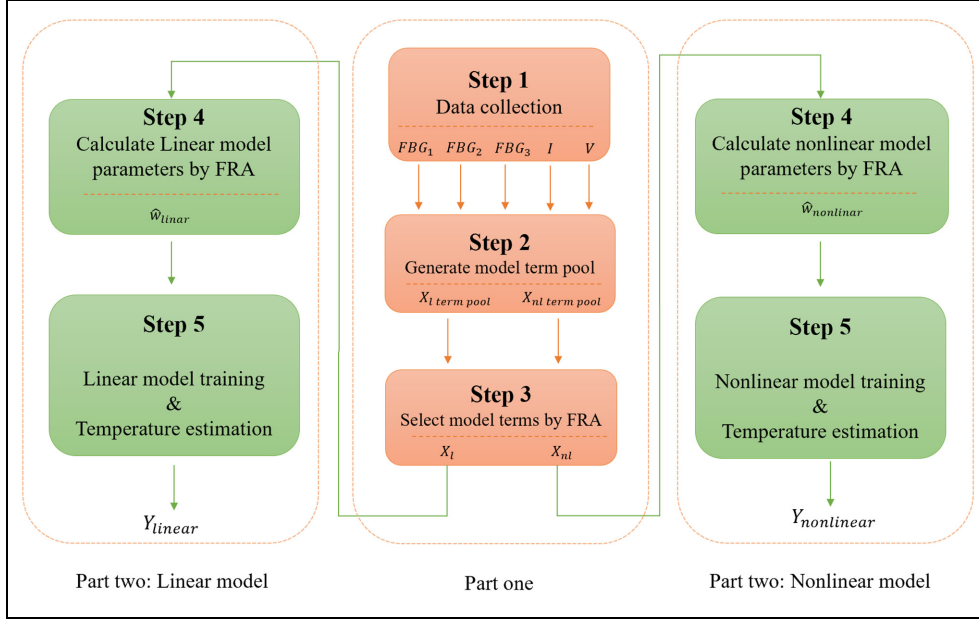


Figure 3. Flowchart of FRA-linear and FRA-nonlinear models.

estimated battery temperature by the linear model. Obviously, the surface temperature prediction evolves smoothly around the actual values. This is essential in some practical applications (e.g. electric vehicles) because the relatively large errors may lead the battery thermal management system to delay taking further actions, thus resulting in a thermal runaway in a brief period. A higher level of compliance between the actual temperature and estimated temperature in Figure 4 leads to small values of MSE and MAE.

The resultant linear model with the linear terms and its identified relevant parameters is provided as follows

$$Y_{\text{linear}} = -3.0885 \times 10^{-7} + 47.873(FBG_2) - 63.238(FBG_1) - 0.36283(V) + 14.882(FBG_3) \quad (24)$$

Equation (24) describes the linear relationship between the independent input variables  $X_l$  and the temperature  $T$ .

**FRA-nonlinear model.** For the nonlinear model, the candidate nonlinear terms are

$$X_{nl \text{ term pool}} = [FBG_1^2, FBG_2^2, FBG_3^2, I^2, V^2, FBG_1^3, FBG_2^3, FBG_3^3, I^3, V^3, FBG_1 \times FBG_2, FBG_1 \times FBG_3, FBG_2 \times FBG_3, FBG_1 \times I, FBG_1 \times V, FBG_2 \times I, FBG_2 \times V, FBG_3 \times I, FBG_3 \times V, I \times V]^T \quad (25)$$

In the first stage, the terms with the largest contribution for the nonlinear model are selected by FRA, as shown below

$$X_{nl} = [FBG_2^3, FBG_2^2, FBG_1^3, I^2, I \times V, I^3, V^3, V^2, FBG_3^3]^T \quad (26)$$

Table 1. The training and testing performance of the FRA-linear model.

Details	Training	Testing
Mean squared error (MSE)	0.0460	0.0514
Mean absolute error (MAE)	0.1684	0.1866

$Y_{\text{train}}$  is the battery surface temperature detected by a thermocouple. The training and testing performances using the FRA-nonlinear model are illustrated in Figure 5. The blue line shows the changes in battery surface temperature read by a thermocouple, whereas the yellow line illustrates the variations of estimated temperature under the nonlinear model.

Furthermore, the training time spent on the FRA-nonlinear model is only 0.0938 seconds. Table 2 provides the error details of both the training and testing results by the FRA-nonlinear model. Especially, the MSE of training and testing are 0.0289 and 0.0317, respectively. And, the MAE of training and testing results are 0.0317 and 0.1447, respectively. The resultant nonlinear model with nonlinear terms and its identified related parameters is given as

$$Y_{\text{nonlinear}} = 9.207 \times 10^{-6}(FBG_2^3) - 0.020111(FBG_2^2) + 3.8523 \times 10^{-6}(FBG_1^3) - 0.050735(I^2) + 0.094943(I^3) + 0.0029075(V^3) - 2.2035 \times 10^{-8}(FBG_3^3) \quad (27)$$

Equation (27) describes the nonlinear relationship between the dependent battery temperature  $T$  as a function of a combination of nonlinear parameters and independent variables  $X_{nl}$ .

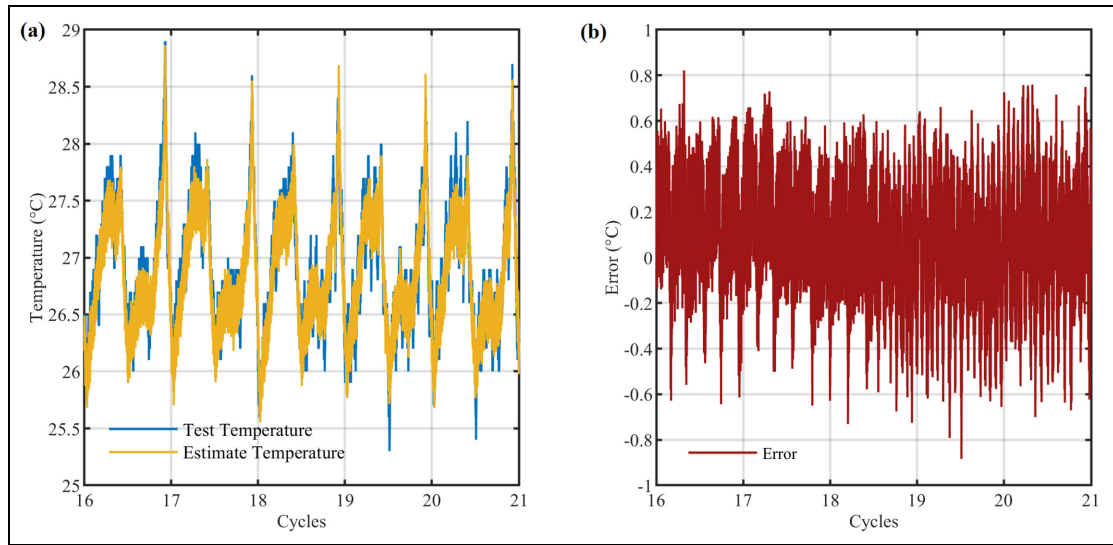


**Figure 4.** Testing performance using FRA-linear model: (a) testing: test temperature versus estimate temperature; (b) error: test temperature–estimate temperature.

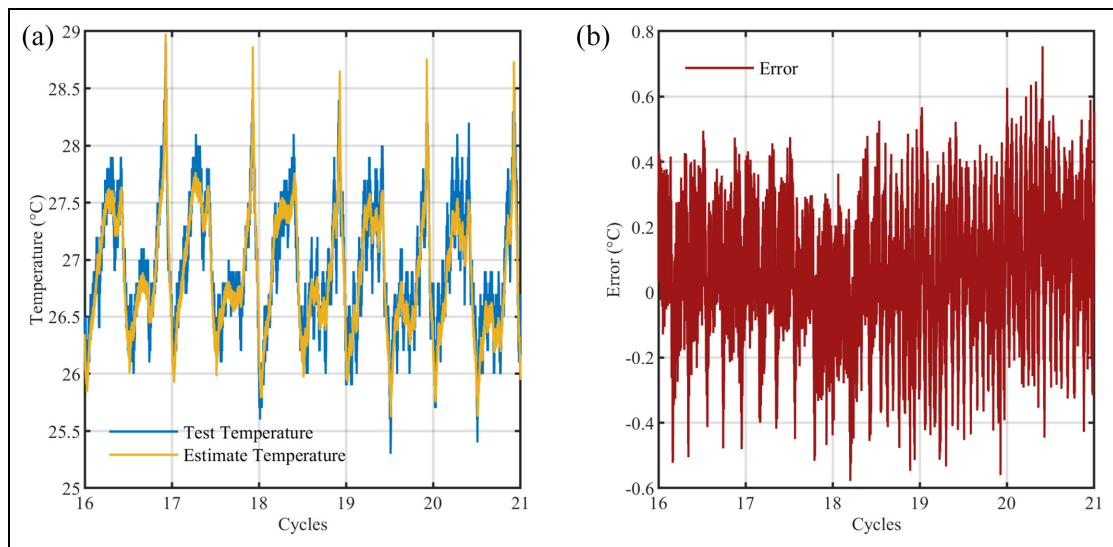


**Figure 5.** Testing performance using FRA-nonlinear model: (a) testing: test temperature versus estimate temperature; (b) error: test temperature–estimate temperature.

**Discussions.** This section provides the battery temperature simulation results based on both the FRA-Linear and FRA-nonlinear models. It is evident that the battery surface

temperature can be accurately estimated via FBG-based data-driven methods. It should be pointed out is that the FRA-nonlinear model spent only 0.0938 seconds on model training compared with 0.1094 seconds by the FRA-linear model. Moreover, the FRA-nonlinear model showed the least training and testing errors, which is inseparable from enough valid inputs.

**Table 2.** The training and testing performance used by FRA-nonlinear model.

Details	Training	Testing
Mean squared error (MSE)	0.0289	0.0317
Mean absolute error (MAE)	0.0317	0.1447

From the simulation results, it is clear that the  $FBG_2$  and its nonlinear terms are chosen by FRA in both the linear and nonlinear models. It means that  $FBG_2$  has close relationship with the temperature (detected by thermocouple). The chosen FBG terms from the three different spots also indicate the

temperature distribution on the surface of battery is nonuniform, though the three spots are close to each other. We can also find that FBG sensors are more sensitive to battery shell temperature changes than the battery cell current and terminal voltage.

## Conclusion and future work

This paper presents the detailed work of exploring the use of FBG sensors and ML to monitor battery temperature. Specifically, 3 FBG sensor signals, terminal voltage, battery current and surface temperature are obtained from a lab experiment setup. In order to improve the accuracy and efficiency of ML models, a two-stage data-driven method is provided.

In the first stage, the inputs with the largest contributions are selected by FRA. Then two different models (i.e. FRA-linear and FRA-nonlinear) are constructed separately. The model testing results show that the methods of integrating FBG sensor data and ML for battery thermal monitoring can predict the battery shell temperature effectively and accurately. For example, with the input data point of (42, 592 × 9), the time spent on the FRA-nonlinear model training is only 0.0938 seconds; the MSE and MAE from model validation are 0.0289 and 0.0317, respectively.

However, it should be noted that the wavelength shifts of three FBG sensors used in the experiment are the results of the temperature changes, strain variations and other factors. We did not extract temperature-induced signals for model training and testing. The experiments conducted were based on the hypothesis that the temperature measurements on the surface of the battery were average values. In fact, the internal and external temperature distribution of the battery or different spots of the battery surface was nonuniform.

The future work will focus on further improvement of the model accuracy so as to effectively and timely detect the internal changes when the temperature and strain information on the battery surface have minor changes, thus enabling the early fault prevention.

## Acknowledgements

S.L. acknowledges the scholarship from the University of Leeds to support his research.


## Declaration of conflicting interests

The author(s) declared no potential conflicts of interest with respect to the research, authorship and/or publication of this article.

## Funding

The author(s) disclosed receipt of the following financial support for the research, authorship and/or publication of this article: This work is partially supported by the SP Energy Network Funded project 'A holistic approach for power system monitoring to support DSO transition'.

## ORCID iDs

Shiyun Liu  <https://orcid.org/0000-0003-4447-9319>

Kang Li  <https://orcid.org/0000-0001-6657-0522>

## References

- Amine K, Liu J and Belharouak I (2005) High-temperature storage and cycling of C-LiFePO<sub>4</sub>/graphite Li-ion cells. *Electrochemistry Communications* 7(7): 669–673.
- Barsoukov E and Macdonald JR (2005) *Impedance Spectroscopy Theory, Experiment, and Applications* (2nd edn). Hoboken, NJ: John Wiley & Sons.
- Elder F and Seefeld P (2015) Self-validating contact thermometry sensors for higher temperatures. *Measurement Science and Technology* 26: 015102.
- Feng X, He X, Ouyang M, et al. (2015) Thermal runaway propagation model for designing a safer battery pack with 25 Ah LiNi Co Mn O<sub>2</sub> large format lithium ion battery. *Applied Energy* 154: 74–91.
- Fleming J, Amietszajew T, McTurk E, et al. (2018) Development and evaluation of in-situ instrumentation for cylindrical Li-ion cells using fibre optic sensors. *HardwareX* 3: 100–109.
- Fortier A, Tsao M, Williard N, et al. (2017) Preliminary Study on Integration of Fiber Optic Bragg Grating Sensors in Li-Ion Batteries and In Situ Strain and Temperature Monitoring of Battery Cells. *Energies* 10: 838.
- Han G, Yan J, Guo Z, et al. (2021) A review on various optical fibre sensing methods for batteries. *Renewable and Sustainable Energy Reviews* 150: 111514.
- Jiang ZY, Li HB, Qu ZG, et al. (2022) Recent progress in lithium-ion battery thermal management for a wide range of temperature and abuse conditions. *International Journal of Hydrogen Energy* 47(15): 9428–9459.
- Kang J, Yan F, Zhang P, et al. (2014) Comparison of comprehensive properties of Ni-MH (nickel-metal hydride) and Li-ion (lithium-ion) batteries in terms of energy efficiency. *Energy* 70: 618–625.
- Karimi D, Behi H, Van Mierlo J, et al. (2022) A comprehensive review of lithium-ion capacitor technology: Theory, development, modeling, thermal management systems, and applications. *Molecules* 27: 3119.
- Lee CY, Lee SJ, Tang MS, et al. (2011) In situ monitoring of temperature inside lithium-ion batteries by flexible micro temperature sensors. *Sensors* 11(10): 9942–9950.
- Li K, Peng J-X and Irwin GW (2005) A fast nonlinear model identification method. *IEEE Transactions on Automatic Control* 50(8): 1211–1216.
- Li Y, Li K, Liu X, et al. (2020) Fast battery capacity estimation using convolutional neural networks. *Transactions of the Institute of Measurement and Control*. Epub ahead of print 5 November. DOI: 10.1177/0142331220966425.
- Li Y, Li K, Liu X, et al. (2021) Lithium-ion battery capacity estimation: A pruned convolutional neural network approach assisted with transfer learning. *Applied Energy* 285: 116410.
- Li Y, Li K, Liu X, et al. (2022) A hybrid machine learning framework for joint SOC and SOH estimation of lithium-ion batteries assisted with fiber sensor measurements. *Applied Energy* 325: 119787.
- Li Z, Zhang J, Wu B, et al. (2013) Examining temporal and spatial variations of internal temperature in large-format laminated battery with embedded thermocouples. *Journal of Power Sources* 241: 536–553.
- Liao Z, Zhang S, Li K, et al. (2019) A survey of methods for monitoring and detecting thermal runaway of lithium-ion batteries. *Journal of Power Sources* 436: 226879.



- Liu K, Li K, Peng Q, et al. (2018) Data-driven hybrid internal temperature estimation approach for battery thermal management. *Complexity* 2018: 1–15.
- Liu K, Li Y, Hu X, et al. (2020) Gaussian process regression with automatic relevance determination Kernel for calendar aging prediction of lithium-ion batteries. *IEEE Transactions on Industrial Informatics* 16(6): 3767–3777.
- Mahamud R and Park C (2022) Theory and Practices of Li-Ion Battery Thermal Management for Electric and Hybrid Electric Vehicles. *Energies* 15: 3930.
- MathWorks (2022) A method for describing nonlinear relationships and making predictions from experimental data. Available at: <https://uk.mathworks.com/discovery/nonlinear-model.html> (accessed 8 June 2022).
- Meyer J, Nedjalkov A, Doering A, et al. (2015) Fiber optical sensors for enhanced battery safety. In: Pickrell G, Udd E and Du HH (eds) *Fiber Optic Sensors and Applications XII*. Bellingham, WA: SPIE. pp. 190–201.
- Morey WW, Meltz G and Glenn WH (1990) Fiber optic Bragg grating sensors. In: Kersey AD, Dakin JP, Dakin JP, et al. (eds) *Fiber Optic and Laser Sensors VII*. Bellingham, WA: International Society for Optics and Photonics. pp. 98–107.
- Nascimento M, Ferreira MS and Pinto JL (2017) Real time thermal monitoring of lithium batteries with fiber sensors and thermocouples: A comparative study. *Measurement* 111: 260–263.
- Nascimento M, Ferreira MS and Pinto JL (2019) Temperature fiber sensing of Li-ion batteries under different environmental and operating conditions. *Applied Thermal Engineering* 149: 1236–1243.
- Novais S, Nascimento M, Grande L, et al. (2016) Internal and external temperature monitoring of a Li-ion battery with fiber Bragg grating sensors. *Sensors* 16: 1394.
- Olabi AG, Maghrabie HM, Adhari OHK, et al. (2022) Battery thermal management systems: Recent progress and challenges. *International Journal of Thermofluids* 15: 100171.
- Raijmakers LHJ, Danilov DL, Eichel RA, et al. (2019) A review on various temperature-indication methods for Li-ion batteries. *Applied Energy* 240: 918–945.
- Ravishanker N, Chi Z and Dey DK (2021) *A First Course in Linear Model Theory*. London: Chapman & Hall/CRC Press.
- Richardson R (2016) *Impedance-based battery temperature monitoring*. PhD Thesis, University of Oxford, Oxford.
- Schwartz J, Arakaki K, Kiesel P, et al. (2015) Embedded fiber optic sensors for in situ and in-operando monitoring of advanced batteries. *MRS Proceedings* 1740: 7–12.
- Wei Z, Hu J, He H, et al. (2022) Embedded distributed temperature sensing enabled multi-state joint observation of smart Lithium-ion battery. *IEEE Transactions on Industrial Electronics* 70: 555–565.
- Wei Z, Zhao J, He H, et al. (2021) Future smart battery and management: Advanced sensing from external to embedded multi-dimensional measurement. *Journal of Power Sources* 489: 229462.
- Xie Y, Yang R, Li W, et al. (2022) A comprehensive study on influence of battery thermal behavior on degradation and consistency. *IEEE Transactions on Transportation Electrification* 8: 3707–3724.
- Yang G, Leitão C, Li Y, et al. (2013) Real-time temperature measurement with fiber Bragg sensors in lithium batteries for safety usage. *Measurement* 46(9): 3166–3172.
- Yang S-O, Lee S, Song SH, et al. (2022) Development of a distributed optical thermometry technique for battery cells. *International Journal of Heat and Mass Transfer* 194: 123020.
- Yu Y, Vergori E, Maddar F, et al. (2022) Real-time monitoring of internal structural deformation and thermal events in lithium-ion cell via embedded distributed optical fibre. *Journal of Power Sources* 521: 230957.
- Zhang L, Liu X, Li K, et al. (2022) Real-time battery temperature monitoring using FBG sensors: A data-driven calibration method. *IEEE Sensors Journal* 22: 18639–18648.